Polystyrene nanoparticles slurry as an additive for developing insulating and waterproof gypsum composites

Daniel López Pedrajas[1], Manuel Carmona Franco[1], I. Garrido Sáenz[2], Francisco J. Ramos Mellado[1], Juan F. Rodríguez Romero[1], Ana M. Borreguero Simón[1*]

[1]*University of Castilla-La Mancha, Department of Chemical Engineering, Institute of Chemical and Environmental Technology. Ciudad Real, Spain.*
[2]*University of Castilla-La Mancha, Department of Applied Mechanics and Engineering Projects, School of Architecture. Toledo, Spain.*
Corresponding author: e-mail: AnaMaria.Borreguero@uclm.es

Abstract

Lightweight gypsum composites with improved thermal and waterproof properties were produced by using a concentrated slurry containing polystyrene nanoparticles (NPS) as an additive. The NPS/Hemihydrate mass ratio was varied between 0.00 and 0.42. The density of the composites decreased with the increase of the NPS/Hemihydrate mass ratio, due to the change in the internal structure to a more lamellar one with crystals of larger size that grow also in a less compact distribution. This also caused an increase of the porosity (from 0.47 to 0.51) and a reduction in the thermal conductivity from 0.354 W m^{-1}K^{-1} (NPS/Hem = 0) to 0.225 W m^{-1}K^{-1} at 32 ºC for the composite manufactured with the maximum NPS amount (NPS/Hem = 0.42). The thermal conductivity decrease allowed to reduce the final temperature at the steady state up to 2.5 ºC compared with the unmodified gypsum, when they were exposed to a heat source at 45 ºC. In addition, it was observed by SEM and TGA that the NPSs were distributed homogeneously throughout the gypsum composites blocks. Although the maximum compressive and flexural strengths decreased with the increase of NPS amount up to 76 and 61 %, respectively; all the synthesized lightweight gypsum blocks satisfied the European standard regulation EN 13279-1. The waterproof properties were measured by the contact angle, passing from 26.2º to 141.5 º when changing from 0.0 NPS/Hem ratio to the maximum amount.

Keywords: lightweight gypsum, thermal conductivity, insulation, porosity, permeability, slurry, waterproof.

Nomenclature

C-NPS/Hem$_x$	Gypsum composites with x = NPS to Hemihydrate mass ratio
DN	Particle size distribution in number
dn$_{0.5}$	Particle size in number
dv$_{0.5}$	Particle size in volume
PDI	Polydispersity Index
FT-IR	Fourier transform infrared
FWHM	Full width at half maximum
Hem	Hemihydrate
HRSEM	High resolution scanning electron microscopy
K	Scherrer constant
k	Thermal conductivity
m_{sample}	Specimen mass
NPS	Polystyrene nanoparticles
q_{acc}	Amount of accumulated heat in the sample
SEM	Scanning electron microscopy
t	Mean size of the crystallite
TES	Thermal energy storage
TGA	Thermogravimetric analysis
VD	Particle size distribution in volume
XRD	X-ray diffraction
ρ_{bulk}	Apparent density
ρ_{real}	Real density
β	Full width at half maximum of the X-ray peak in radians minus the instrumental width
ε	Porosity
Λ	Wavelength of the Cu-Kα radiation
Θ	Bragg angle
$\lvert \zeta \rvert$	Zeta potential

1. Introduction

The growing increase in energy demand is becoming a real problem in modern society, in terms of the environment (due to greenhouse gas emissions) and of the availability of energy resources [1]. The building sector is responsible of the 40 % of energy consumption and of the 36 % of CO_2 emissions in the European Union [2]. Consequently, governments have implemented a series of regulations and directives with the aim of renovating the housing stock, prioritizing energy efficiency by improving the thermal insulation or applying new building designs and promoting the use of sustainable energy resources [3,4].

The improvement of the construction materials thermal insulation is getting great importance in terms of energy saving in building sector. The main goal is to obtain materials with high porosity in order to decrease their thermal conductivity [5,6]. Air-entrance agents and foaming agents can be used to get that target. Also, several kinds of additives or lightweight aggregates can be added in building materials composites to get the same effect. In bibliography, there are many lightweight composite materials; containing diverse kinds of additives such as pumice [7], diatomite [8], expanded vermiculite [9], expanded perlite [10], expanded clay [11], fly ash [12], oil palm shell [13], rubber [14], expanded polystyrene [15,16], waste plastics [9,17,18] and encapsulated phase change material [19,20], among others [21–23].

One of the most widely used materials in the building sector is gypsum, due to its low cost and the fact that it is a very versatile compound. It has been traditionally used in ceiling and wall claddings, which are key areas of energy losses in buildings [24]. Therefore, the way of improving its insulating capacity, while keeping the rest of its properties almost intact, is being extensively studied. Borreguero *et al.* [19] manufactured lightweight gypsum composites with improved thermal energy storage capacity by adding different kind of microencapsulated phase change materials with a polymeric shell. They incorporated up to a 15 wt% of capsules with respect to the hemihydrate (Hem), obtaining a reduction in the thermal conductivity up to 25.8 %, with an increase in the thermal energy storage capacity up to 63.88 %. In addition, all the lightweight gypsum composites that they manufactured complied with the standard European regulation EN 13279-1 [25]. Thompson *et al.* [21] fabricated a hierarchically porous gypsum composite by the incorporation of micro-size agar hydrogel in the recipe formulation of the material. They achieved an increase in the porosity up to 60 % with a reduction in the thermal

conductivity from 0.42 W m^{-1}K^{-1} (unmodified gypsum) to 0.20 W m^{-1}K^{-1}. Nevertheless, the mechanical properties of the new porous and insulating composite were much worse than the unmodified gypsum. On the other hand, gypsum composites, prepared from flue gas desulfurization binder and different kinds of fillers (silica sand, perlite, expanded clay aggregate and waste polyurethane foam), were manufactured by Doleželová et al.[22]. By adding these fillers, they achieved an increase in the porosity from 30.4 to 61.3 % with a decrease in the thermal conductivity from 1.8 to 0.2 W m^{-1}K^{-1}, in compliance with the standard European regulation EN 13279-1 [25]. Nevertheless, the samples with lightweight aggregates accumulated a higher amount of water and did it faster. Bouzit *et al.* [16] introduced expanded polystyrene balls (3-5 mm) in the manufacture of plasters, generating an increase in their porosity as well as a decrease in their thermal conductivity. However, there was a large decrease in the maximum compressive strength of lightweight gypsum composites with the increase in the number of polystyrene beads.

On the other hand, it is well known that water is one of the most aggressive external atmospheric agents that penetrates building materials structure causing an important physical and chemical degradation, what compromises its functionality. In this regard, the improvement of the building material waterproof properties by adding a layer of polymer or other hydrophobic materials such as SiO_2-CH_3, or by incorporating them in the manufacture of the material, has been studied by several authors [26–30]. The addition of layers involves an extra step in the final material production and the layer effectiveness can be reduced with the pass of time due to its thickness reduction or partial damages, not lasting the whole building lifetime. Additionally, the homogeneous incorporation of hydrophobic fillers throughout the gypsum composites is not easily achieved, due to the presence of water as reagent for the gypsum manufacturing that can promote the agglomeration of the hydrophobic filler. Thus, further materials or a better incorporation of those previously tested must be tried for the development of lightweight gypsum composites. For this purpose, a slurry concentrated in polystyrene nanoparticles (NPS) has been used as an additive, in order to change the properties of the gypsum, decreasing its thermal conductivity and improving its waterproof properties, while agreeing with the rest of requirements of building regulations. To the best of our knowledge, the use of slurries concentrated in nanoparticles of polystyrene functionalized with hydroxyl groups (-OH) by means of tetraorthosilicate and vinyltriethoxysilane, for the manufacture of gypsum composites exhibiting hydrophobic properties and low

thermal conductivity has not been studied up to now. Thus, the addition of a NPS slurry instead of dry nanoparticles is a novel approach that facilitate the homogeneous distribution of the NPS throughout the entire gypsum specimens thanks to the way the particles are dispersed in it. Besides, the water of the slurry is used as settling water. The physical, chemical and thermal properties, as well as the waterproof ones of all the composites manufactured were studied; demonstrating that this method generates materials with improved insulating and waterproof properties that comply with current regulations for use in the building sector.

2. Materials and methods

2.1. Materials

Gypsum plaster for coatings, supplied by BigMat S.A., and milli-Q water, with a conductivity value lower than 5 μS cm^{-1}, were used for fabricating the lightweight gypsum blocks. The properties of the gypsum plaster for coatings employed are gathered in Table 1. The slurry concentrated in polystyrene nanoparticles was synthesized following our previous recipe [31]. The slurry used as an additive for the manufacturing of gypsum composites was one highly concentrated in polystyrene nanoparticles, with low viscosity and non-Newtonian behavior [31], whose values of solids content, zeta potential ($|\zeta|$) and particle size in volume and number ($dv_{0.5}$ and $dn_{0.5}$, respectively) are listed in Table 2. For the synthesis of the slurry, the suspension polymerization method was employed, using sodium dodecyl sulfate as surfactant. Besides, the polystyrene nanoparticles were functionalized with tetraorthosilicate and vinyltriethoxysilane, in order to increase the stability of the colloidal suspension.

2.2. Lightweight gypsum blocks manufacturing

Gypsum blocks were synthesized by weighting first the mass of the slurry needed for obtaining the desired NPS/Hemihydrate (NPS/Hem) mass ratio and then, completing with the amount of water required to achieve a mass ratio water/Hem of 0.6. Then, the mass of Hem was mixed with the slurry and water using a mixer that satisfies the European regulation UNE-EN 196-1 [32]. The mixing process was carried out at slow speed (rotation movement of 140 min^{-1} and planetary movement of 62 min^{-1}) for 1.5 min. Finally, the mixture was poured into a mold of 40×40×160 mm for the mechanical test,

5

to a mold of 30×60×100 mm for the thermal analysis and to a mold of 20×110×110 mm for studying the thermal conductivity in lambdometer. All specimens were dried at room temperature for one week and then at 40 ºC until complete evaporation of the water excess, in accordance with the European Standard regulation EN 13279-2. The composites are named as C-NPS/Hem$_x$, where "x" is the NPS/Hem mass ratio. The recipes used for the manufacturing of the C-NPS/Hem are shown in Table 3.

2.3. Lightweight gypsum blocks characterization

2.3.1 Density and porosity

The bulk density of the gypsum blocks (ρ_{bulk}) was determined by weighing and sizing the dry specimens. The real density (ρ_{real}) was determined by helium pycnometry (Micromeritics Accupy II 1340). The porosity of the gypsum composites (ε) was calculated with the Eq. 1 from the ρ_{bulk}, ρ_{real} and assuming that the gypsum pores are filled by air which remains trapped into the gypsum once it solidifies. The air density (ρ_{air}) was assumed to be 1.186 kg m^{-3}, which corresponds to the ρ_{air} at 25 ºC and 1 atm.

$$\varepsilon = \frac{\rho_{real} - \rho_{bulk}}{\rho_{real} - \rho_{air}} \qquad [1]$$

2.3.2. Scanning Electron Microscopy (SEM) analysis

Manufactured gypsum composites were depicted by means of Scanning Electron Microscopy (SEM) by using a Quanta 250 (FEI Company) with a tungsten filament operating at a working potential of 15 to 20 kV. The Backscattered Electron Detector (BSED) was applied for imaging. The SEM equipment was equipped with an Apollo X EDX from AMETEK, an energy dispersive X-ray spectrometer (EDX), which analyzed the chemical composition with detection limits between 1000 ppm and 0.1 wt%.

2.3.3. X-Ray Diffraction (XRD) analysis

The crystallography of the obtained materials was analyzed by using a Bruker D8 Advance X-ray reflectometer, with θ - θ configuration, Cu-Kα radiation, Gobel mirror to produce parallel beam, special sample holder for reflectivity measurements, 0D point scintillation detector and at the same time 1D LynxEye detector.

2.3.4. Fourier Transform Infrared (FT-IR) spectroscopy

Fourier Transform Infrared (FT-IR) spectroscopy analysis was carried out on a Spectrum Two spectrometer (Perkin Elmer, Inc) equipped with a Universal Attenuated Total Reflectance (UATR) accessory. Three samples in different positions of the same specimen were carried out (at 0, 20 and 40 mm of mechanical test specimen). The infrared spectra were collected using 16 scans and 16 cm^{-1} resolution in the wavelength range of 4000 to 500 cm^{-1}.

2.3.5. Mechanical tests

The mechanical properties of the lightweight gypsum composites were studied by using a Servohydraulic Test System (MTS Criterion Model 43). The flexion and compressive strengths were obtained according to standard UNE-EN 13279-2 [33]. The flexion tests were done using specimens of 40×40×160 mm applying a load rate of 50 N s^{-1} until fracture. The compression tests were done using the broken flexion test specimens. A load rate of 1 N mm^{-2}s^{-1} was applied over 40×40 mm surface load application until fracture.

2.3.6. Contact angle

The contact angle analyses were performed on gypsum specimens of 30×60×100 mm. Three measurements were done in different points of the same specimen to obtain the average value. The tests were carried out with an Attension Theta Optical Tensiometer from Biolin Scientific´s, with a computer controlled by OneAttension software and provided with a high-definition camera.

2.3.7. Thermogravimetric Analyses (TGA) of gypsum composites

The thermal stability of the synthesized composites was analyzed by Thermogravimetric analysis (TGA) using a SDT Q600 Simultaneous DSC-TGA (TA Instruments). Three samples from different positions of the same specimen (taken at 0, 20 and 40 mm from the edge of the mechanical test specimens) were tested in order to study the homogeneity of the composites. Temperature was tuned from room temperature to 700 ºC, under a nitrogen atmosphere and using a heating rate of 10 ºC min^{-1}.

2.3.8. Lambdometer

A lambdometer model HFM 446 Lambda medium (NETZSCH) was used in order to quantify the thermal conductivity of the manufactured lightweight gypsum. The HFM 446 uses the heat flow meter method based in the following standards: ISO 8301, ASTM

C 518, DIN EN 12667, JIS A 1412, DIN EN 12664 and ASTM C 1784. With this method the specimens are tested between two heat flux sensors in fixed or adjustable temperature gradients. After a few minutes for the system to reach the equilibrium, the software computer determines the thermal conductivity and thermal resistance of the sample. It uses a steady-state measurement process. The specimens are in contact with the upper and lower plates, which are stabilized at two different temperatures. Due to the temperature gradient imposed, heat flows vertically through the specimen, from hot face to cold face. These plates are equipped with heat flux transducer and peltier system in order to keep constant the temperature and heat flow. The values of heat flow and temperature are used to calculate the specimen thermal conductivity under steady-state conditions.

The thermal conductivities of the manufactured specimens with dimensions of 110×110×20 mm were measured at 8, 16, 24, 28, 32, 40 and 45 ℃ with a temperature gradient of 20 ℃ between upper and bottom plates. The tests were performed three times using for that the same specimen.

2.3.9. Procedure and experimental equipment for the thermal behavior tests of the composite gypsum blocks

The thermal behavior of the gypsum composites has been studied using a homemade equipment designed in the Chemical Engineering Department of the University of Castilla-La Mancha. With this equipment, the temperature profiles at different positions of the specimens are registered with time while they are subjected to a cold or hot source (only in one of their faces) passing from one steady state to another. The equipment consisted of an aluminum cell of 30×60×100 mm and wall thickness of 1 mm, through which a liquid coming from a thermostatic bath is pumped. The temperature of the aluminum cell is controlled with the temperature of this liquid. The lightweight gypsum composites specimens are placed on the cell and further insulated with foams boards of 4 cm in thickness. A more exhaustive description of the equipment and proofs of its successful performance for the thermal characterization of materials can be found in previous works [20,34–36].

In this work, tests were carried out applying set-point step changes from 18 to 45 ± 0.1 ℃ in the thermostatic bath. Six thermocouples of K-type were used to measure temperatures: two were put in the external test specimen surface (T_{up}), other two at the

8

middle of the specimen (T_{middle}) and the last ones on the cell surface (T_{down}). The liquid flow was high enough (9 L h^{-1}) to ensure the absence of thermal profile in liquid direction. Six heat flow sensors gSKIN®-XI and gSKIN®-XP were putted on the six faces of the test specimens in order to monitor online the inlet and outlet heat fluxes. Fig. 1 shows the distribution of the thermocouples and heat flow sensors in the studied specimen. Thermocouples and heat flow sensors signals were registered continuously using the NOKEVAL program and recorded by means of a computer.

Three samples of each synthesized gypsum were tested.

3. Results and discussions

3.1. Physical properties

The ρ_{real}, ρ_{bulk} and ε (Equation 1) were obtained by employing the specimens used for the mechanical tests, after completely dried. As can be seen in Fig. 2, the ρ_{bulk} and ρ_{real} densities linearly decreased with the NPS content (between 1315.6 - 942.3 kg m^{-3} and 2488.0 – 1925.0 kg m^{-3}, respectively), but agreeing in all cases with the standard regulation UNE EN-13279-1 for binders and gypsum plasters, since all the ρ_{bulk} were higher than the limit value of 600 kg m^{-3} [25]. This density decrease can be partially attributed to the fact that NPS have a lower density (1097.7 kg m^{-3}) than gypsum (2488.0 kg m^{-3}). Thus, the higher the NPS/Hem ratio, the lower the apparent and real densities. However, when determining the theoretical density of the manufactured gypsum composites by means of the linear mixing rule (Table 4), this is always higher than the real one (ρ_{real}); increasing the difference with the NPS content. This is due to the increase of the gypsum crystals size or morphology changes which drive to a less compact structure, what can also justify the increase of the porosity of the synthesized gypsum specimens with the NPS content. In order to confirm this hypothesis, SEM pictures and XRD analyses of gypsum composites were done. The SEM pictures of the internal gypsum composites' structure are shown in Fig. 3.

It can be seen in Fig. 3 that the gypsum without NPS showed a morphology of very thin rectangular prisms, being able to agglomerate and form a compact structure. However, by increasing the amount of NPS with respect to the hemihydrate, the crystals showed a more lamellar structure, more clustering and larger cross section size caused by crystals condensation. Therefore, increasing the NPS/Hem mass ratio resulted in less compact structure and caused a decrease in density and an increase in porosity. The areas

marked by circles are the nanoparticles occupying the pores, located thanks to the SEM backscattered detector. The detector makes it possible to distinguish the nanoparticles, with lower density, (blurred darker areas) and the gypsum crystals, with higher density (brighter white areas). In addition, it has been included an EDX picture of the C-NPS/Hem$_{0.42}$, where the zones occupied by the gypsum crystals (green color) and the NPS (red color) are clearly differentiated. In conclusion, it has been demonstrated that the addition of NPS to the gypsum matrix results in a less dense structure, thus, producing an increase in the porosity of the specimens. Besides, SEM pictures and EDX results allowed to conclude that there are NPS distributed through the whole gypsum.

Fig. 4 shows the XRD analysis of the gypsum composites manufactured with different amounts of NPS. In order to determine the mean size (t) of the ordered crystalline domains in the manufactured gypsum blocks, the Debye-Scherrer formula has been employed:

$$t = \frac{K \times \lambda}{\beta \times cos\theta} \qquad [2]$$

where t is the mean size of the crystallite, K is the Scherrer constant and taken equal to 0.9, λ is the wavelength of the Cu-Kα radiation (1.54056 Å), β is the Full Width at Half Maximum (FWHM) of the X-ray peak in radians minus the instrumental width and θ is the Bragg angle [37].

In Fig. 4a, it is observed that all the gypsum composites are mainly constituted by crystalline monoclinic calcium sulfate dihydrates ($CaSO_4 \cdot 2H_2O$), they showed very clear and narrow peaks principally located at 2θ = 11.6º, 20.7º, 23.4º, 29.1º, 31.1º, 33.3º, 35.9º, 40.6º, 43.5º, 47.9º, 50.3º and 51.3º. It also can be seen vestiges of unreacted orthorhombic hemihydrate ($CaSO_4 \cdot \frac{1}{2}H_2O$) in the peak at 2θ = 32.85º, being a bit more pronounced for the gypsum without NPS (C-NPS/Hem$_0$).

In Fig. 4b, it can be seen how the FWHM decreased with the increase of the NPS/Hem mass ratio, revealing an increase of the crystallinity and domain size as the dose of NPS is increased. The FWHM changed from 0.135 for C-NPS/Hem$_0$ to 0.109 in the case of the lightweight gypsum with the maximum load in NPS (C-NPS/Hem$_{0.42}$). The t (Equation 2) of the crystallite varies from 1971.4 to 2903.4 nm, confirming the trend of crystallinity enhancement with the NPS/Hem mass ratio. These XRD findings were in

good agreement with the tendency observed in SEM images (Fig. 3), since the higher the NPCS load, the higher the crystallite size of the matrix gypsum composites structures.

To confirm the presence of the NPS in the composite gypsum blocks, FT-IR spectroscopy analyses were performed in CO_2 at three different positions of a specimen for each NPS/Hem mass ratio. The media of the FT-IR spectra of the gypsum composites and the FT-IR spectrum of the pure NPS are shown in Fig. 5. The FT-IR spectra of the NPS presented the absorption bands at 3020, 750 and 695 cm-1, attributed to aromatic C-H stretching vibration, corresponding to the polystyrene [38–40] and bands corresponding to Si-alkoxy and Si-OH groups at 1110-1000 and 920-850 cm^{-1}, respectively [31]. In addition, peaks located in 1490 and 1450 cm^{-1} confirmed the presence of aromatic C=C stretching vibration absorption [41]. In the spectrum of gypsum without NPS, the band within 3200 - 3800 cm^{-1} denotes asymmetric stretching band of water remained into gypsum. The band observed at 1150 cm^{-1} represented the symmetric stretching vibration of -OH groups from water. Besides, the band recorded at 1619 cm^{-1} was attributed to the bending vibration of S-O group in $CaSO_4$ [42,43]. The spectra of the gypsum composites with NPS presented the characteristic bands of the polystyrene and the pure gypsum, demonstrating, undoubtedly, that the NPSs were part of the gypsum matrix.

3.2. Mechanical properties

Flexural and compression tests were performed on gypsum specimens added with the polystyrene nanoparticles in order to determine their influence in maximum breaking stress, both in flexural and compression. For this purpose, specimens with dimensions 4×4×160 mm were used. The tests were carried out in accordance with the European standard regulation UNE-EN 13279-2 [33]. Fig. 6 shows the results obtained for these tests. It can be seen that both, the maximum flexural and compressive ultimate stresses, followed the same trend; decreasing as the NPS/Hem mass ratio increased, up to 61 and 76 %, respectively. This effect is due to the previously commented change in the crystal morphology (crystals of larger size that grow also in a less orderly distribution), caused by the addition of the NPS, what drives to a less compact structure. In addition, it can be also partially attributed to the fact that polystyrene has lower flexural and compressive strengths (0.3 and 0.1 MPa, respectively) [44] than C-NPS/Hem_0 (4.9 and 13.2 MPa, respectively). In the case of the maximum flexural strength (Fig. 6a), it became practically

constant from the NPS/Hem mass ratio of 0.2. This means that the mechanical energy absorption of the specimen increases with the increase of polystyrene in the gypsum matrix. On contrary, in the maximum compression strength test (Fig. 6b), it was observed a significant decrease in this mechanical property for NPS/Hem mass ratio of higher than 0.3. Nevertheless, it is remarkable to say that both, the flexural and compression properties, comply with the European standard regulation UNE-EN 13279-1 [25].

3.3. Waterproof properties

Since the slurry used in this research for the manufacture of lightweight gypsum composites consists of polystyrene nanoparticles (hydrophobic material) stabilized with the help of Si-based cosurfactant [31], it is expected to achieve an improvement of the material hydrophobicity. The waterproofing ability of the surfaces is characterized by the water droplet contact angle technique, which is visually quantifiable by measuring the angle that forms a water drop with the tested surface [45]. The contact angle of the lightweight gypsum composites was measured at 3 different points of the same specimen in the side that was on the mold side, which is smooth and regular; in order to reduce the effect of the surface morphology (Fig. 7).

Fig. 7a shows the average contact angle of the lightweight gypsum synthesized with different NPS/Hem mass ratio. It can be observed how the addition of a 0.1 of NPS with respect of the hemihydrate produced a considerable improvement in the waterproof properties of the newly synthesized composite, as the contact angle increases from 26.2° (C-NPS/Hem$_0$) to 106.1° (C-NPS/Hem$_{0.1}$), achieving an increase in contact angle of up to 4.4 times for C-NPS/Hem$_{0.42}$. Furthermore, this effect is observed to occur across the entire surface of the material, since a maximum standard deviation of only ± 11.3° was obtained for C-NPS/Hem$_{0.2}$. In Fig. 7b, it is represented the droplet aged of the synthesized lightweight gypsum with the maximum amount of NPS (C-NPS/Hem$_{0.42}$). It can be observed that the contact angle was practically constant during the 2 first min of the test, thereafter, there was a reduction in the contact angle until reaching a value of 87.9°. It is important to note that during the 5 min of the droplet aging test the contact angle is always above 26.2° of the C-NPS/Hem$_0$. Finally, Fig. 7c shows more visually the waterproof properties enhancement, since C-NPS/Hem$_0$ absorbs water droplets from practically the first moment they were added to the surface of the specimen, while in the case of C-NPS/Hem$_{0.42}$ they remain on the surface of it for a prolonged time. Moreover, this experiment was carried out 2 years after the production of the specimen, indicating

that this property is maintained over time. It has been reported in bibliography a contact angle between 90º and 165 º by using polymer or Si based product in the building material [26,28–30]. However, these materials tend to present low energy efficiency [45].

3.4. Thermal properties

In order to know the thermal stability of the manufactured composites gypsum blocks with different amount of NPS and to know if the NPS were homogeneously distributed throughout the gypsum matrix, TGAs were carried out on the specimens used for the mechanical tests in three different positions (40, 20 and 0 mm). The results obtained are shown in Fig. 8. In Fig. 8a, the TGA curve of the C-NPS/Hem$_0$ presented three regions of weight loss. The first one, observed between 80 and 160 ºC, is attributed to the evaporation of the absorbed water (hygroscopic water) and the chemically bound water of the hydrated salt. The second one, that occurs between 510 and 550 ºC, corresponds to the release of the water bound to hydraulic compounds ($CaSO_4 \cdot 2H_2O$ and $CaSO_4 \cdot \frac{1}{2}H_2O$) and the last one, the smallest one (starting close to 700ºC), refers to the CO_2 formed during the decomposition of carbonates [46–48]. The PSS TGA curve presented three steps of weight loss [31]. The first one, between room temperature and 100 ºC, corresponds to the fluid phase evaporation (water); the second one, at *ca.* 220 ºC, corresponds to the dispersant degradation (SDS), and the last one, at *ca.* 400 ºC can be attributed to the polystyrene degradation [49]. Finally, a 0.8 wt% remains none degraded at 700 ºC due to the inorganic content of the SDS and the cosurfactant based on VTES and TEOS. The TGA curves of the gypsum composites with different NPS/Hem mass ratio showed four clear weight losses due to the absorbed water (between 80 and 160 ºC), the SDS (*ca.* 220 ºC), the NPS (*ca.* 400 ºC) and the water bound to hydraulic compounds (between 510 and 550 ºC). The NPS content present in each composite according to the TGA results is shown in Table 5. The NPS content is equal to the weight loss that occurs around 400 ºC, since NPS is formed from polystyrene and, as explained before, the degradation of this polymer occurs at this temperature. It is worthy to point out that the biggest deviation, between the three TGA in the different points of the specimens, was only a 0.90 wt% for C-NPS/Hem$_{0.3}$. In addition, the three TGA measurements are within the confidence interval for an alpha = 0.10. So, at this point, it is possible to say, without any doubt, that the NPS have a good distribution in the composite when it is added in the form of homogeneous and stable slurry. Fig. 8b shows, as an example, the TGA curves of the synthesized composite gypsum with the maximum NPS load (C-NPS/Hem$_{0.42}$),

where the mentioned homogeneity is demonstrated.

In order to know if the change in the porosity and the presence of NPS in the gypsum composites affected to their thermal behavior, a measurement of the thermal conductivity (k) of all the manufactured specimens were carried out by using a lambdometer. Measurements were made at 8, 16, 24, 28, 32, 40 and 45 °C, in order to have a scanning at different temperatures (Fig. 9). As can be observed in Fig. 9, the k of the gypsum composites blocks decreased with the increase of the NPS/Hem mass ratio. The thermal conductivity of C-NPS/Hem$_0$ was 0.353 ± 0.005 W m^{-1}K^{-1} at 32 °C and decreased to 0.258 ± 0.004, 0.253 ± 0.004, 0.236 ± 0.021 and 0.225 ± 0.011 W m^{-1}K^{-1} when the NPS/Hem mass ratio increased from 0.10 to 0.20, 0.30 and 0.42, corresponding to a decrease of a 27.0, 28.4, 33.4 and 36.3 % in the k, compared with that of C-NPS/Hem$_0$, respectively. All the k values of the manufacture specimens at different temperatures are shown in Table 5. The decrease of the k with the NPS presence can be attributed to the porosity increase due to the following factors: a) the increase of porosity involves an increase of air inside the composite gypsum blocks and air is an excellent thermal insulator (0.026 W m^{-1}K^{-1}) compared to the solid phase [5]; b) the presence of a porous structure increased the conduction interfaces between the gypsum phase and thermal phonons, thereby increasing the interfacial thermal resistance [6]. Besides, this drop in k is also due to the lower thermal conductivity of NPS (0.105 - 0.128 W m^{-1}K^{-1}) [50] compared to unmodified gypsum (0.304 - 0.340 W m^{-1}K^{-1}). It was found that this improvement in the insulating properties was similar and even better than that from other gypsum composites synthesized by using polymers as additives, in order to increase its porosity. Bicer et al. [15] added up to a 80 % in volume of expanded polystyrene into a composite, achieving an improvement in the thermal conductivity of 17 % with a reduction in the compressive strength of 40 %. Bouzit et al. [16] manage to obtain a conductivity value of 0.116 W m^{-1}K^{-1} by adding 30 wt% of expanded polystyrene balls of 3 mm diameter, however, these gypsum composites do not comply with European standards in terms of mechanical properties. On the other hand, Borreguero et al.[19] achieved a reduction in the thermal conductivity up to 16 % by the addition of a 15 wt% of polystyrene microcapsules into a gypsum composite.

It was also observed a slight decrease of the thermal conductivity of pure gypsum with temperature, mainly from 30°C. This agrees with the behavior observed by previous researchers that attribute this reduction to the moisture presence [51–53]. The thermal

conductivity reduction was higher when NPS was used, which can be related to an excess of moisture due to the use of the NPS.

On the other hand, this kind of materials tend to have poor waterproof properties due to the increase in the porosity. However, this is not the case of the developed composites, thanks to the hydrophobicity of the incorporated NPS. In light of these results, this kind of composite gypsum blocks by using a concentrated NPS slurry could be a promising candidate for thermal insulation in the edification sector.

As commented before, the thermal behavior was also studied by a homemade equipment that allows to measure the temperature profiles and inlet and outlet heat flows of the gypsum blocks when they are subjected to a heating or cooling process. Fig. 10 shows the temperature profiles of the external face of the lightweight gypsum manufactured with different NPS/Hem mass ratio when they are subjected to a heating process from 18 to 45 ºC using for that homemade experimental equipment. This temperature would be the one inside the building when it is subjected to high external temperatures. It is observed that as the amount of NPS in the building material increases, the temperature that reaches the external face of the specimen in the steady state is lower. It is obtained up to a temperature reduction of 2.5 ºC for the case of C-NPS/Hem$_{0.42}$ with respect to C-NPS/Hem$_0$. This temperature reduction with the addition of the NPS slurry is due to the modification of the structure of the gypsum matrix generating a more porous materials with a lower thermal conductivity, as previously demonstrated; also due to the lower thermal conductivity of NPS with respect to gypsum. Thus, materials with better insulating properties have been obtained.

4. CONCLUSIONS

The use of a slurry concentrated in NPS allowed to develop lightweight gypsum with a maximum NPS/Hem mass ratio of 0.42 with a synergetic improvement in the waterproof and insulating properties. The use of the slurry facilitated the homogeneous distribution of the NPSs throughout the lightweight gypsum, according to SEM pictures and EDX and TGA results. The density of the composites decreased with the increase of the NPS/Hemihydrate mass ratio, due to a change in the morphology of the gypsum crystals to a more lamellar one with bigger sizes, which promoted less compact structures, causing an increase in their porosity. The increase in the porosity, together with the low thermal conductivity of the NPS compared to gypsum, increase the insulating capacity of

the gypsum, with a reduction in the thermal conductivity of the new material from 0.354 to 0.225 W m^{-1}K^{-1} when using a NPS/Hem mass ratio of 0.42. Moreover, the addition of NPSs in the fabrication of lightweight gypsum blocks generated an increase in the water contact angle of 4.4 times for the 0.42 NPS/hemihydrate mass ratio, demonstrating the improvement in the waterproof properties. Regarding the mechanical properties, although the maximum compressive and flexural strength decreased with the increase of NPS load, all of the synthesized lightweight gypsum composites satisfied the European standard regulation EN 13279-1 for gypsum binders and plasters, since all of them presented flexural and compressive strengths above 1 and 2 MPa, respectively.

Acknowledgements

References

[1] U.S. Energy Information Administration, How much carbon dioxide is produced per kilowatthour of U.S. electricity generation?, (2020). https://www.eia.gov/tools/faqs/faq.php?id=74&t=11.

[2] European Parliament (2018) Directive (EU) 2018/ of the European Parliament and of the Council of 30 May 2018 amending Directive 2010/31/EU on the energy performance of buildings and Directive 2012/27/EU on energy efficiency., (n.d.).

[3] State Secretary for Transport, Mobility and Urban Agenda. ERESEE 2020. 2020 update of the long-term strategy for energy rehabilitation in the Spain building sector., (2020).

[4] C.V. Podara, I.A. Kartsonakis, C.A. Charitidis, Towards phase change materials for thermal energy storage: classification, improvements and applications in the building sector, Appl. Sci. 11 (2021) 1–26. https://doi.org/10.3390/app11041490.

[5] Y.S. Touloukian, R.W. Powell, C.Y. Ho, M.C. Nicolaou, Thermophysical properties of mather - The TPRC Data Series. Volume 10. Thermal Diffusivity, Thermophys. Electron. Prop. Inf. Anal. Cent. Lafayette In. (1974).

[6] Y.H. Kim, Y.W. Kim, W.S. Seo, Processing and properties of silica-bonded porous nano-SiC ceramics with extremely low thermal conductivity, J. Eur. Ceram. Soc. 40 (2020). https://doi.org/10.1016/j.jeurceramsoc.2019.11.072.

[7] N. Degirmenci, A. Yilmaz, Use of pumice fine aggregate as an alternative to standard sand in production of lightweight cement mortar, Indian J. Eng. Mater. Sci. 18 (2011) 61–68.

[8] O. Ünal, T. Uygunoğlu, A. Yildiz, Investigation of properties of low-strength lightweight concrete for thermal insulation, Build. Environ. 42 (2007) 584–590. https://doi.org/10.1016/j.buildenv.2005.09.024.

[9] F. Koksal, E. Mutluay, O. Gencel, Characteristics of isolation mortars produced with expanded vermiculite and waste expanded polystyrene, Constr. Build. Mater. 236 (2020) 117789. https://doi.org/10.1016/j.conbuildmat.2019.117789.

[10] M. Lanzón, P.A. García-Ruiz, Lightweight cement mortars: Advantages and inconveniences of expanded perlite and its influence on fresh and hardened state

and durability, Constr. Build. Mater. 22 (2008) 1798–1806. https://doi.org/10.1016/j.conbuildmat.2007.05.006.

[11]   C. Muñoz-Ruiperez, A. Rodríguez, S. Gutiérrez-González, V. Calderón, Lightweight masonry mortars made with expanded clay and recycled aggregates, Constr. Build. Mater. 118 (2016) 139–145. https://doi.org/10.1016/j.conbuildmat.2016.05.065.

[12]   O. Kayali, Fly ash lightweight aggregates in high performance concrete, Constr. Build. Mater. 22 (2008) 2393–2399. https://doi.org/10.1016/j.conbuildmat.2007.09.001.

[13]   P. Shafigh, M.Z. Jumaat, H. Mahmud, Oil palm shell as a lightweight aggregate for production high strength lightweight concrete, Constr. Build. Mater. 25 (2011) 1848–1853. https://doi.org/10.1016/j.conbuildmat.2010.11.075.

[14]   M. del Río Merino, J. Santa Cruz Astorqui, M.G. Cortina, Viability analysis and constructive applications of lightened mortar (rubber cement mortar), Constr. Build. Mater. 21 (2007) 1785–1791. https://doi.org/10.1016/j.conbuildmat.2006.05.014.

[15]   A. Bicer, F. Kar, The effects of apricot resin addition to the light weight concrete with expanded polystyrene, J. Adhes. Sci. Technol. 31 (2017) 2335–2348. https://doi.org/10.1080/01694243.2017.1299974.

[16]   S. Bouzit, F. Merli, M. Sonebi, C. Buratti, M. Taha, Gypsum-plasters mixed with polystyrene balls for building insulation: Experimental characterization and energy performance, Constr. Build. Mater. 283 (2021) 122625. https://doi.org/10.1016/j.conbuildmat.2021.122625.

[17]   L. Gu, T. Ozbakkaloglu, Use of recycled plastics in concrete: A critical review, Waste Manag. 51 (2016) 19–42. https://doi.org/10.1016/j.wasman.2016.03.005.

[18]   M.K. Mondal, B.P. Bose, P. Bansal, Recycling waste thermoplastic for energy efficient construction materials: An experimental investigation, J. Environ. Manage. 240 (2019) 119–125. https://doi.org/10.1016/j.jenvman.2019.03.016.

[19]   A.M. Borreguero, I. Garrido, J.L. Valverde, J.F. Rodríguez, M. Carmona, Development of smart gypsum composites by incorporating thermoregulating

microcapsules, Energy Build. 76 (2014) 631–639. https://doi.org/10.1016/j.enbuild.2014.03.005.

[20] A.M. Borreguero, A. Serrano, I. Garrido, J.F. Rodríguez, M. Carmona, Polymeric-SiO$_2$-PCMs for improving the thermal properties of gypsum applied in energy efficient buildings, Energy Convers. Manag. 87 (2014) 138–144. https://doi.org/10.1016/j.enconman.2014.07.027.

[21] B.R. Thompson, T.S. Horozov, S.D. Stoyanov, V.N. Paunov, Hierarchically porous composites fabricated by hydrogel templating and viscous trapping techniques, Mater. Des. 137 (2018) 384–393. https://doi.org/10.1016/j.matdes.2017.10.046.

[22] M. Doleželová, L. Scheinherrová, J. Krejsová, M. Keppert, R. Černý, A. Vimmrová, Investigation of gypsum composites with different lightweight fillers, Constr. Build. Mater. 297 (2021) 123791. https://doi.org/10.1016/j.conbuildmat.2021.123791.

[23] X. Ding, S. Wang, R. Dai, H. Chen, Z. Shan, Hydrogel beads derived from chrome leather scraps for the preparation of lightweight gypsum, Environ. Technol. Innov. 25 (2022) 102224. https://doi.org/10.1016/j.eti.2021.102224.

[24] L. Zalewski, S. Lassue, B. Duthoit, M. Butez, Study of solar walls - Validating a simulation model, Build. Environ. 37 (2002) 109–121. https://doi.org/10.1016/S0360-1323(00)00072-X.

[25] AENOR, Standard UNE-EN 13279-1. Gypsum binders and gypsum plasters. Part 1: Definitions and requirements., (2009).

[26] R. Ramachandran, K. Sobolev, M. Nosonovsky, Dynamics of droplet impact on hydrophobic/icephobic concrete with the potential for superhydrophobicity, Langmuir. 31 (2015) 1437–1444. https://doi.org/10.1021/la504626f.

[27] N. Sakthieswaran, M. Sophia, Effect of superplasticizers on the properties of latex modified gypsum plaster, Constr. Build. Mater. 179 (2018) 675–691. https://doi.org/10.1016/j.conbuildmat.2018.05.150.

[28] P. Ma, C. Wang, Y. Gao, X. Gu, B. Cheng, Z. Fang, G. Xiong, J. Wu, The Coupling Effect of Organosilicon Hydrophobic Agent and Cement on the Water Resistance

of Phosphogypsum, Materials (Basel). 15 (2022) 845. https://doi.org/10.3390/ma15030845.

[29] I. Izarra, J. Cubillo, A. Serrano, J.F. Rodriguez, M. Carmona, A hydrophobic release agent containing SiO2-CH3 submicron-sized particles for waterproofing mortar structures, Constr. Build. Mater. 199 (2019) 30–39. https://doi.org/10.1016/j.conbuildmat.2018.12.018.

[30] Y. Zhao, Y. Liu, Q. Liu, W. Guo, L. Yang, D. Ge, Icephobicity studies of superhydrophobic coatings on concrete via spray method, Mater. Lett. 233 (2018) 263–266. https://doi.org/10.1016/j.matlet.2018.09.008.

[31] D. López-Pedrajas, A.M. Borreguero, F.J. Ramos, M. Carmona, J.F. Rodríguez, The role of vinyl terminated silanes for producing highly concentrated polystyrene slurries in a single step process, Colloid Polym. Sci. 298 (2020) 1685–1697. https://doi.org/https://doi.org/10.1007/s00396-020-04754-w.

[32] OFICEMEN, Standard UNE-EN 196-1. Methods of testing cement. Part 1: Determination of strength, (2018) 1–40.

[33] AENOR, Standard UNE-EN 13279-2. Gypsum binders and gypsum plasters. Par2: Test methods, (2014).

[34] A.M. Borreguero, M. Luz Sánchez, J.L. Valverde, M. Carmona, J.F. Rodríguez, Thermal testing and numerical simulation of gypsum wallboards incorporated with different PCMs content, Appl. Energy. 88 (2011) 930–937. https://doi.org/10.1016/j.apenergy.2010.08.014.

[35] C. Barreneche, A. De Gracia, S. Serrano, M. Elena Navarro, A.M. Borreguero, A. Inés Fernández, M. Carmona, J.F. Rodriguez, L.F. Cabeza, Comparison of three different devices available in Spain to test thermal properties of building materials including phase change materials, Appl. Energy. 109 (2013) 544–552. https://doi.org/10.1016/j.apenergy.2013.02.061.

[36] A. Serrano, A.M. Borreguero, I. Garrido, J.F. Rodríguez, M. Carmona, Reducing heat loss through the building envelope by using polyurethane foams containing thermoregulating microcapsules, Appl. Therm. Eng. 103 (2016) 226–232. https://doi.org/10.1016/j.applthermaleng.2016.04.098.

[37]   A.L. Patterson, The scherrer formula for X-ray particle size determination, Phys. Rev. 56 (1939) 978–982. https://doi.org/10.1103/PhysRev.56.978.

[38]   M. Barholin, G. Boissier, J. Dubois, Styrene-divinylbenzene copolymers, 3. Revisited IR analysis., Die Makromol. Chemie. 7 (1981) 2875–2085. https://doi.org/https://doi.org/10.1002/macp.1981.021820719.

[39]   A.M. Szczotok, M. Carmona, A.-L. Kjøniksen, J.F. Rodriguez, The role of radical polymerization in the production of thermoregulating microcapsules or polymers from saturated and unsaturated fatty acids, J. Appl. Polym. Sci. 135 (2018) 45970. https://doi.org/10.1002/app.45970.

[40]   R. Salgado-Pizarro, J.A. Padilla, E. Xuriguera, C. Barreneche, A.I. Fernández, Novel shape-stabilized phase change material with cascade character: Synthesis, performance and shaping evaluation, Energies. 14 (2021) 2621. https://doi.org/10.3390/en14092621.

[41]   J. Fang, Y. Xuan, Q. Li, Preparation of polystyrene spheres in different particle sizes and assembly of the PS colloidal crystals, Sci. China Technol. Sci. 53 (2010). https://doi.org/10.1007/s11431-010-4110-5.

[42]   E. Knittle, W. Phillips, Q. Williams, An infrared and Raman spectroscopic study of gypsum at high pressures, Phys. Chem. Miner. 28 (2001) 630–640. https://doi.org/10.1007/s002690100187.

[43]   A. Karaipekli, A. Sarı, A. Biçer, Thermal regulating performance of gypsum/(C18–C24) composite phase change material (CPCM) for building energy storage applications, Appl. Therm. Eng. 107 (2016) 55–62. https://doi.org/10.1016/j.applthermaleng.2016.06.160.

[44]   N. Pérez, G. Paul, G. Anguas, A.P. Salazar, R. Juárez, H. Federico, C. Mondragón, Evaluation of the mechanical properties of expanded polystyrene, Mex. Transp. Inst. (2016) 79.

[45]   H. Boostani, S. Modirrousta, Review of Nanocoatings for Building Application, in: Procedia Eng., 2016: pp. 1541–1548. https://doi.org/10.1016/j.proeng.2016.04.194.

[46]   A. Greco, A. Maffezzoli, O. Manni, Development of polymeric foams from

recycled polyethylene and recycled gypsum, Polym. Degrad. Stab. 90 (2005) 256–263. https://doi.org/10.1016/j.polymdegradstab.2005.01.026.

[47]   M. Anastasiou, T. Hasapis, T. Zorba, E. Pavlidou, K. Chrissafis, K.M. Paraskevopoulos, TG-DTA and FTIR analyses of plasters from byzantine monuments in Balkan region : Comparative study, J. Therm. Anal. Calorim. 84 (2006) 27–32. https://doi.org/10.1007/s10973-005-7211-9.

[48]   D.A. Kontogeorgos, D.I. Kolaitis, M.A. Founti, Numerical modeling of heat transfer in gypsum plasterboards exposed to fire, Conf. 6th Int. Conf. Heat Transf. Fluild Mech. Thermodyn. (2008).

[49]   G. Chigwada, E. Kandare, D. Wang, S. Majoni, D. Mlambo, C.A. Wilkie, J.M. Hossenlopp, Thermal stability and degradation kinetics of polystyrene/organically- modified montmorillonite nanocomposites, J. Nanosci. Nanotechnol. 8 (2008) 1927–1936. https://doi.org/10.1166/jnn.2008.027.

[50]   J.E. Mark, Polymer data handbook, New York: Oxford University Press, 1999.

[51]   A.C.J. De Korte, H.J.H. Brouwers, Calculation of thermal conductivity of gypsum plasterboards at ambient and elevated temperature, Fire Mater. 34 (2010). https://doi.org/10.1002/fam.1009.

[52]   N. Benichou, C. Canada, M.A. Sultan, C. Canada, Thermal Properties of Wood , Gypsum and Insulation at Elevated Temperatures . Internal Report, NRC Publ. Arch. (2001).

[53]   I. Rahmanian, Thermal and mechanical properties of gypsum boards and their influences on fire resistance of gypsum board based systems, University of Manchester, 2011.

Figure captions

Fig. 1. Heat flow sensors and thermocouples distribution in the homemade equipment for studying the gypsum composites thermal behavior.

Fig. 2. ρ_{bulk}, ρ_{real} and ε of the manufacture composite gypsum blocks with different NPS/Hem mass ratio.

Fig. 3. SEM images of gypsum composites with different PS/Hem mass ratio. The lower right image is an EDX mapping of C-NPS/Hem$_{0.42}$, where the green color corresponds to Ca from gypsum and the red color to C from NPS.

Fig. 4. a) X-Ray Diffraction patterns of the manufactured gypsum composites. b) Full width at half maximum (FWHM) and corresponding mean size of the crystallite (t) obtained for the main peak located at $2\theta = 11.6\,^{\circ}$ using the Debye-Scherrer (Eq. 3) formula for the gypsum composites prepared with different NPS/Hem mass ratio.

Fig. 5. FT-IR analyses of the manufactured gypsum composites and the pure NPS.

Fig. 6. a) Flexural and b) compression strengths of the gypsum blocks as function of NPS/Hem mass ratio.

Fig. 7. a) Contact angle of the lightweight gypsum composites with different NPS/Hem mass ratio and b) evolution of the contact angle with time of the C-NPS/Hem$_{0.42}$. c) Comparison of hydrophobicity of lightweight gypsum composites by using NPS slurry as additive in a 0.42 NPCS/Hem and without it after 2 years.

Fig. 8. a) Average TGA curves of the composite gypsum blocks with different NPS/Hem mass ratio and b) TGA curves of samples at different position of the C-NPS/Hem$_{0.42}$.

Fig. 9. Thermal conductivity of the manufactured composite gypsum blocks with different NPS/Hem mass ratio at different temperatures by using a lambdometer.

Fig. 10. a) Temperature profiles of the external surface and b) the accumulative power of the lightweight gypsum with different NPS/Hem mass ratio when they are subjected to a heating process from 18 to 45 ºC.
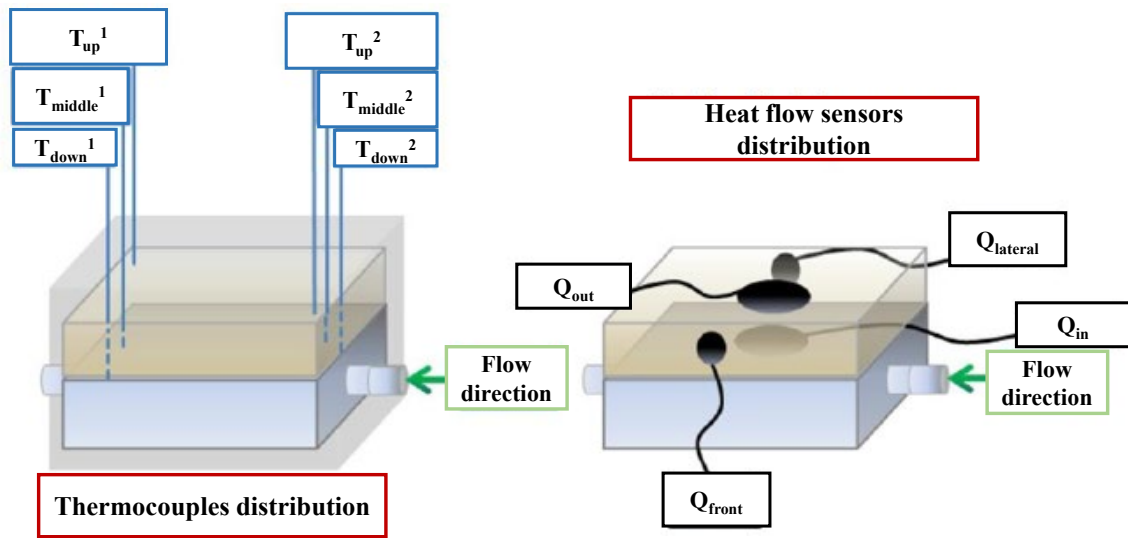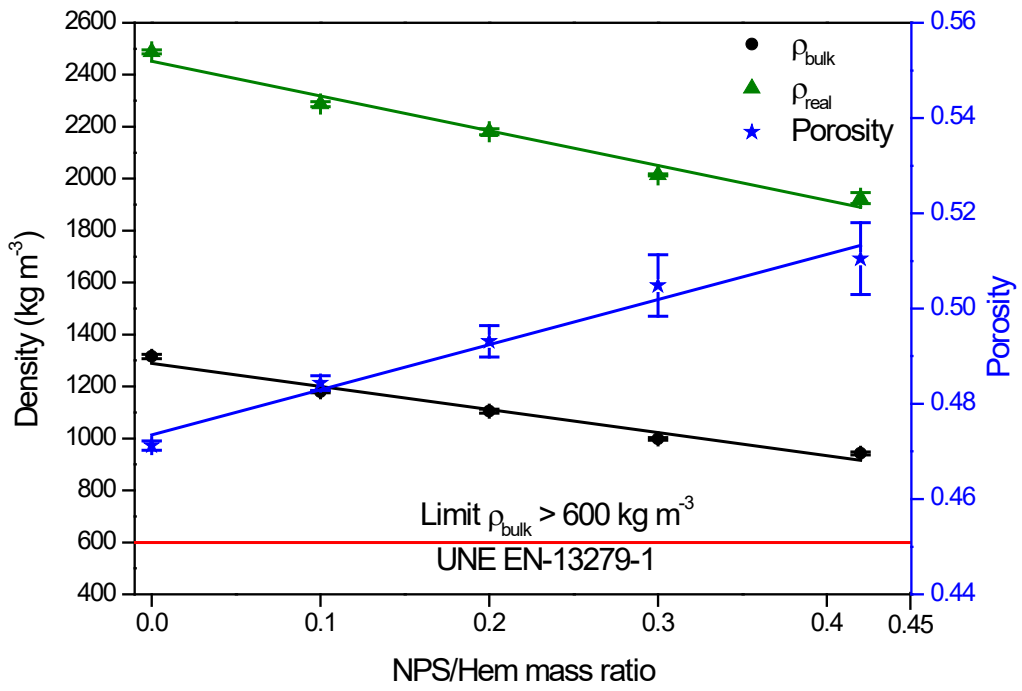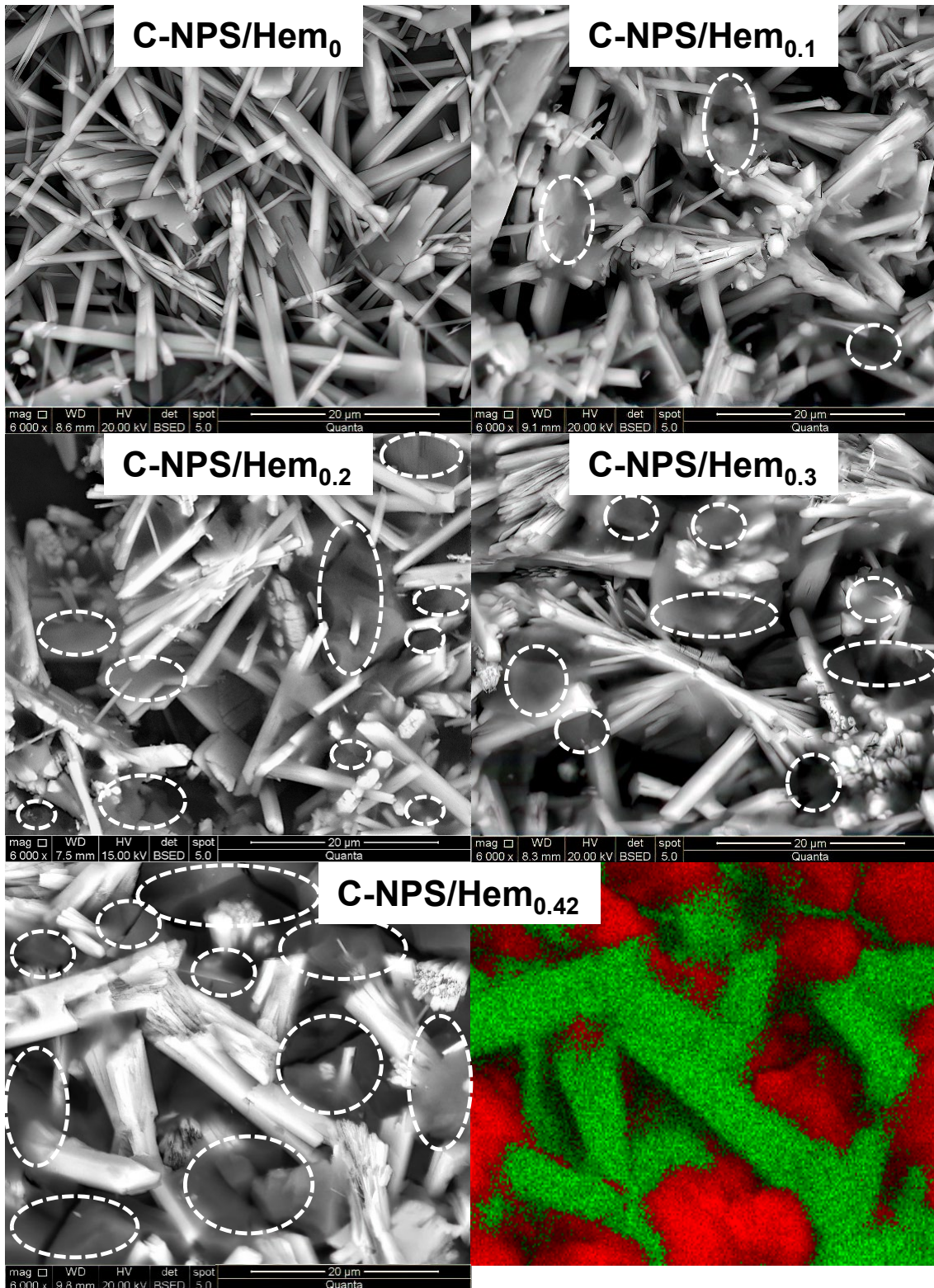
Figure 1

T_{up}^{1}

T_{middle}^{1}

T_{down}^{1}

T_{up}^{2}

T_{middle}^{2}

T_{down}^{2}

Heat flow sensors distribution

$Q_{lateral}$

Q_{out}

Q_{in}

Flow direction

Flow direction

Thermocouples distribution

Q_{front}

Figure 2

Figure 3

Figure 4
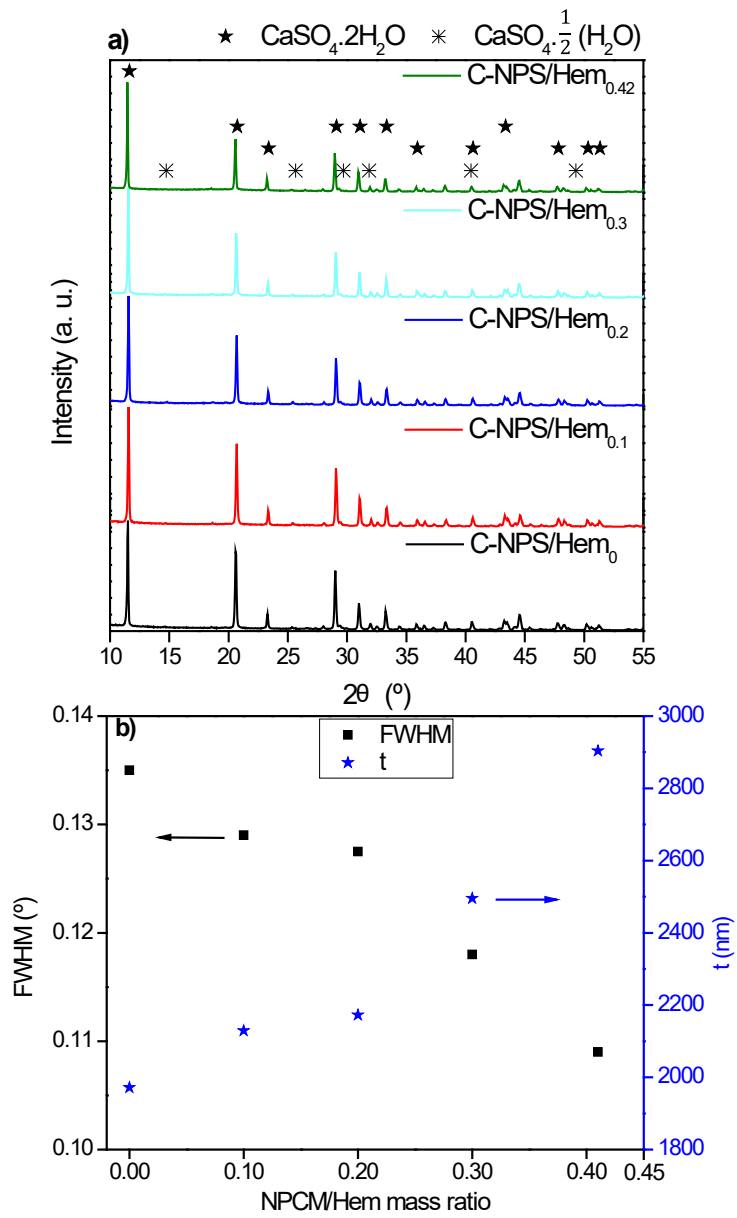
Figure 5
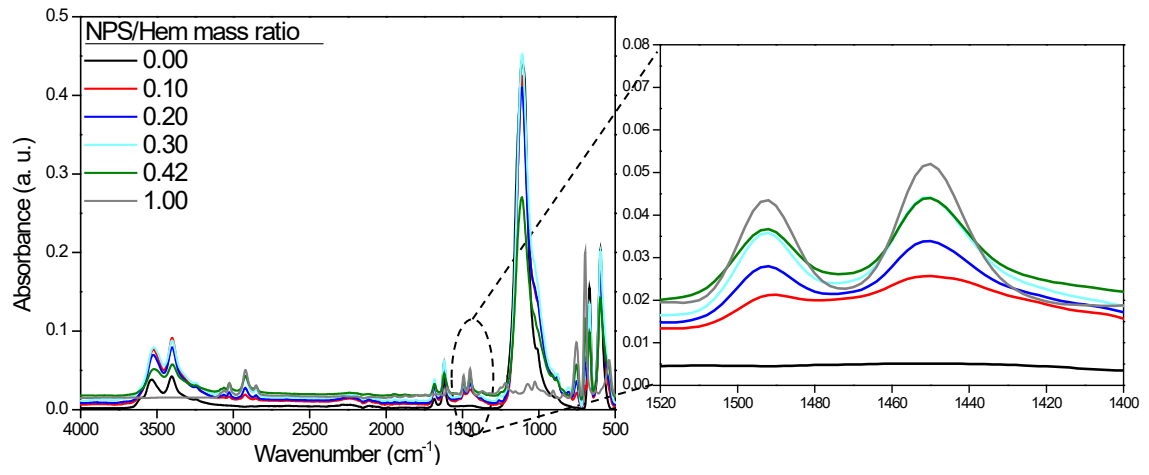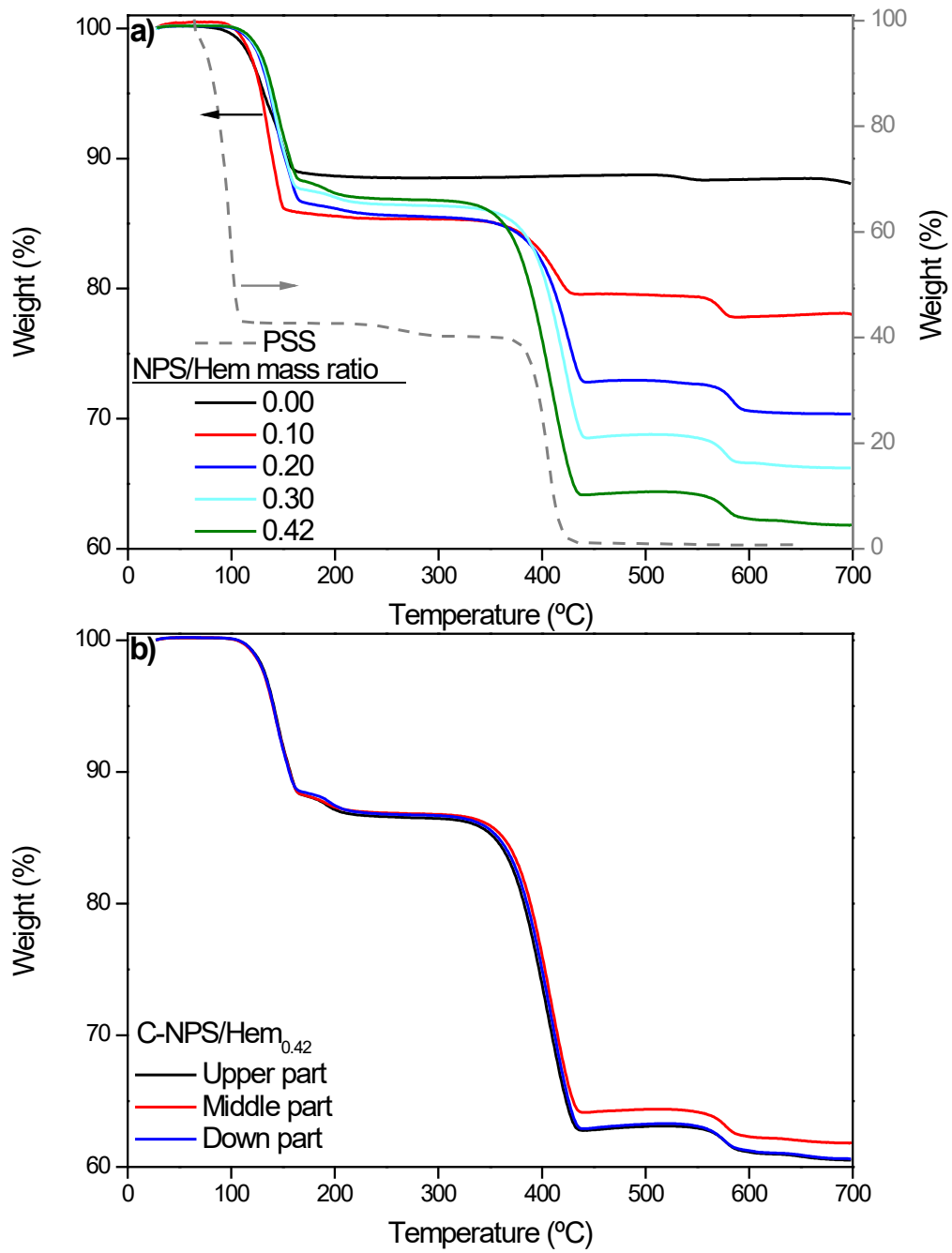
Figure 6
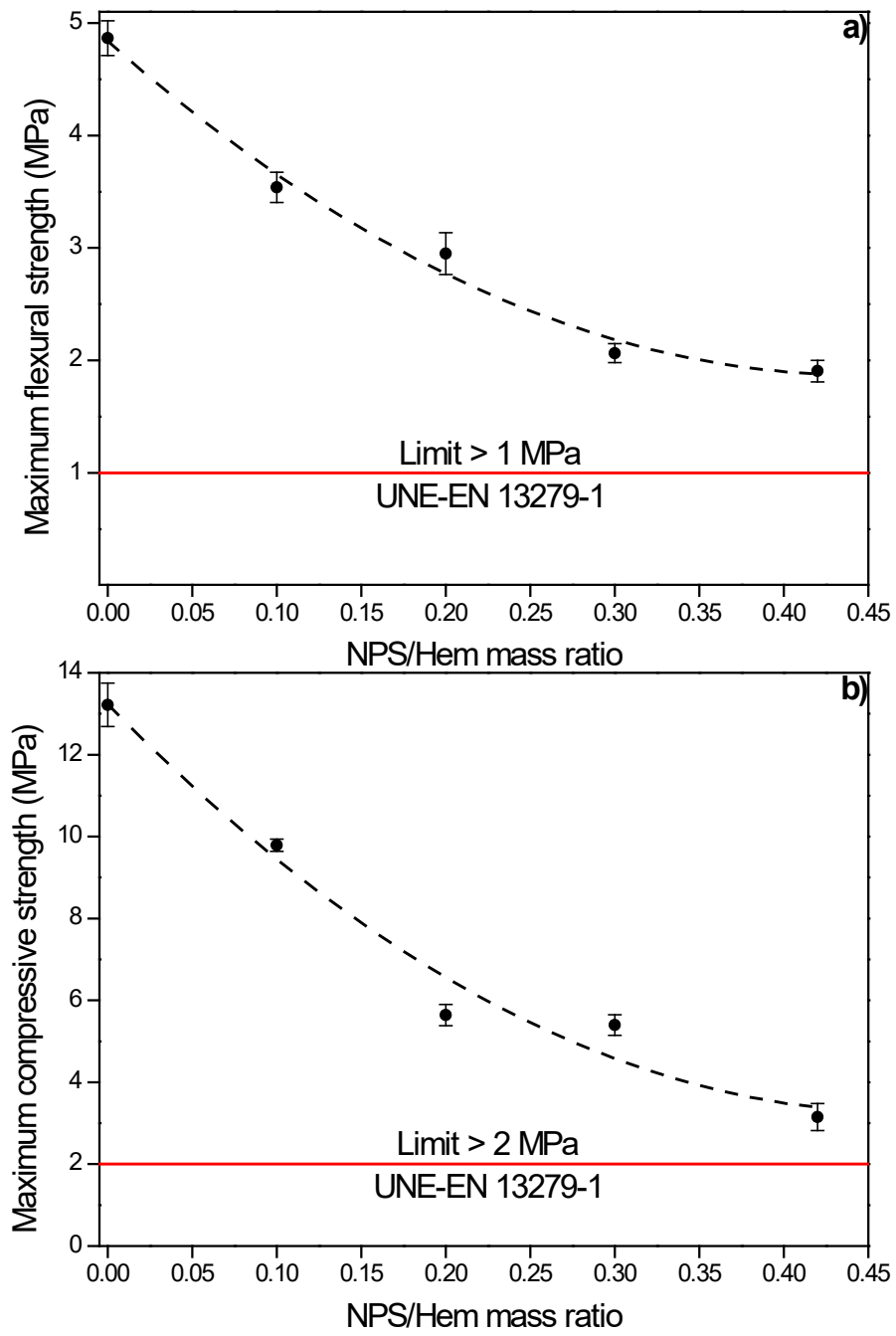
Figure 7
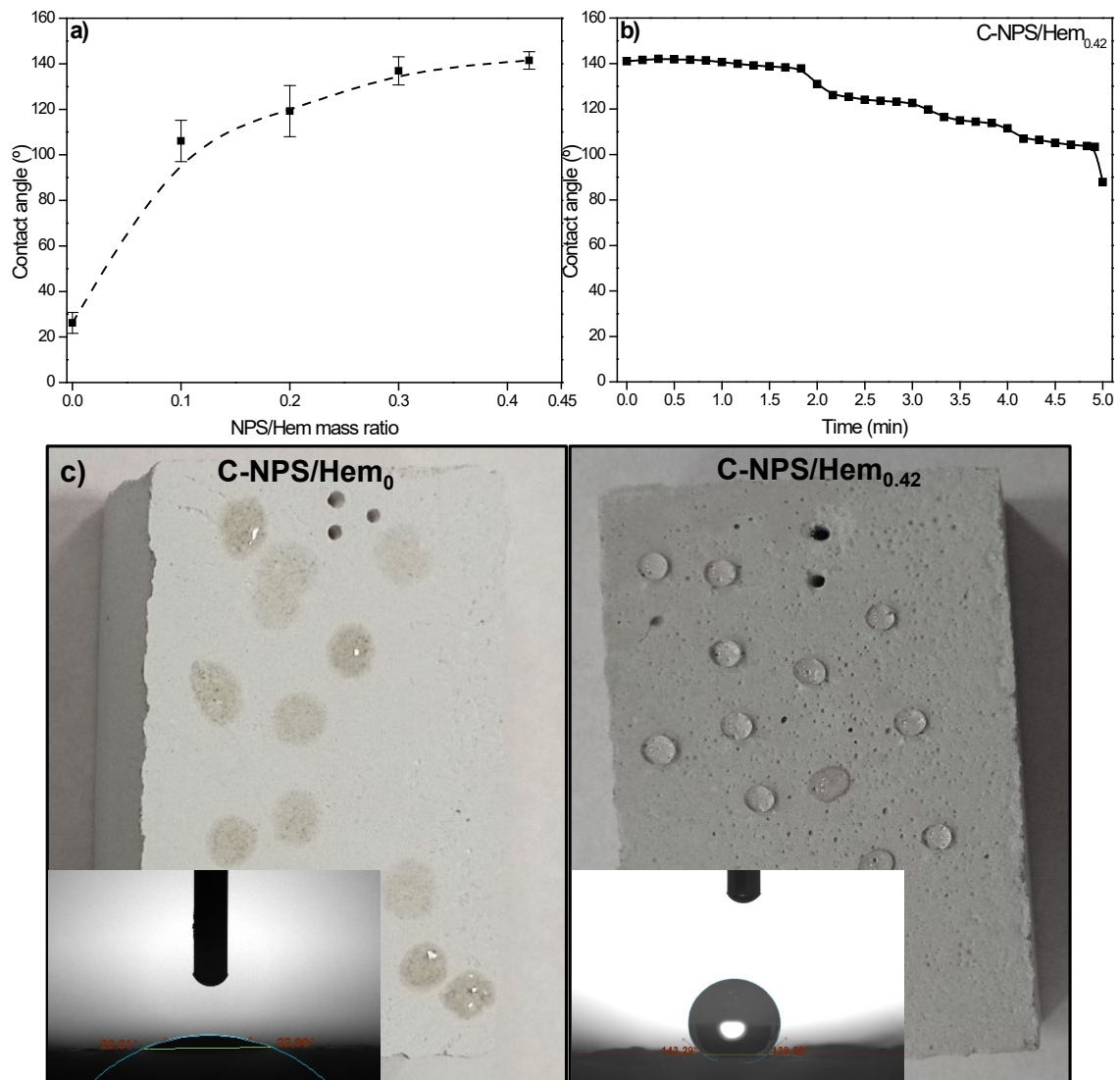
Figure 8

Figure 9
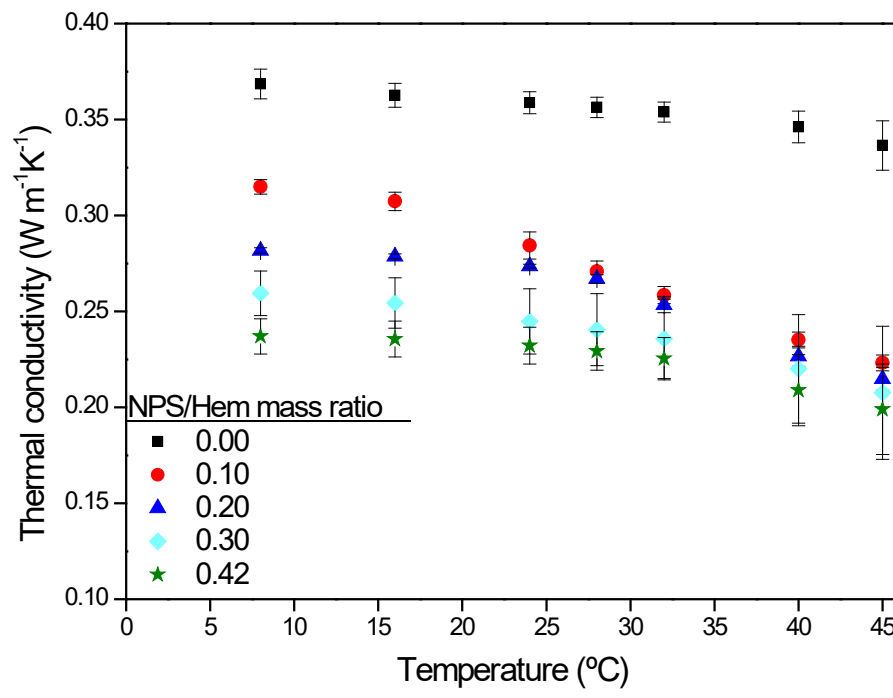
Figure 10
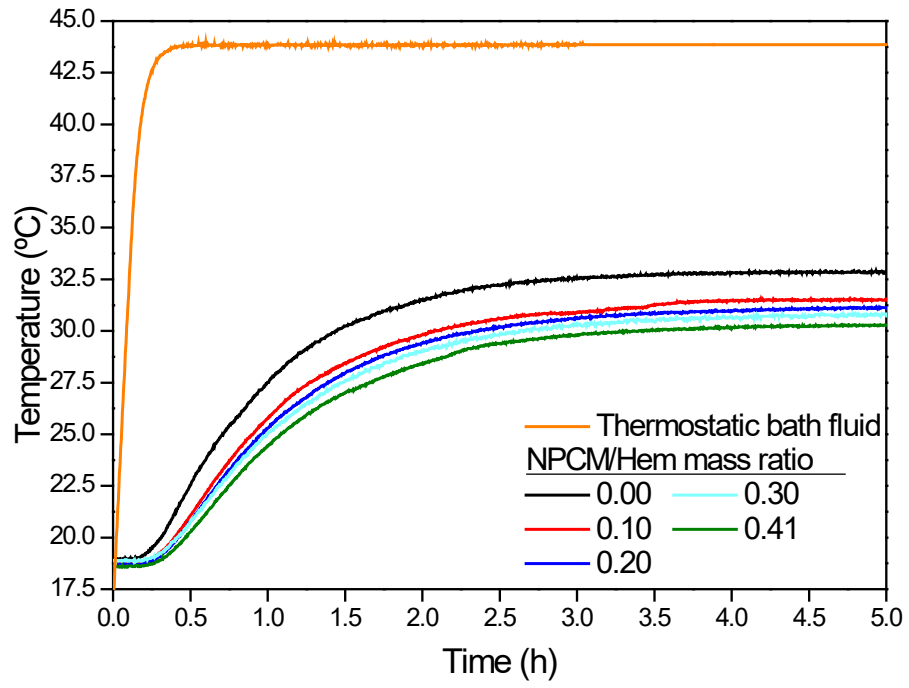
Table 1. Properties of the gypsum plaster for coating used for the lightweight gypsum fabrication.

Combined water	4.5 - 5 %
Sulphur trioxide	45 - 50 %
pH	10
Purity index	≥ 85 %
Granulometry	Gross

Table 2. Solids content, viscosity at share rates of 1 and 680 s^{-1}, $|\zeta|$ and $dv_{0.5}$, $dn_{0.5}$ and PDI of the used NPS slurry.

Solids content (wt%)	μ at share rates 1-680 s^{-1} (mPa s)	$|\zeta|$ (mV)	$dv_{0.5}$ (nm)	$dn_{0.5}$ (nm)	PDI
39.4	127.6-37.6	53.3	75.3	64.0	0.047

Table 3. Weight mass percentage of hemihydrate, slurry and water in the manufactured composites.

	Hem (wt%)	Slurry (wt%)	Water (wt%)
C-NPS/Hem$_0$	62.5	0.0	37.5
C-NPS/Hem$_{0.1}$	58.8	14.3	26.9
C-NPS/Hem$_{0.2}$	55.6	27.0	17.4
C-NPS/Hem$_{0.3}$	52.6	38.4	9.0
C-NPS/Hem$_{0.42}$	49.5	50.5	0.0

Table 4. Real and theoretical densities and deviation between them.

	Real density (kg m^{-3})	Theoretical density (kg m^{-3})	|Deviation| (%)
C-NPS/Hem$_0$	2488.0	2488.0	-
C-NPS/Hem$_{0.1}$	2287.0	2404.6	4.9
C-NPS/Hem$_{0.2}$	2180.0	2315.0	5.8
C-NPS/Hem$_{0.3}$	2015.0	2241.1	10.1
C-NPS/Hem$_{0.42}$	1925.0	2162.7	11.0

Table 5. NPS content in the three TGA measurements of the same specimen and the average, standard deviation and error for an Alpha = 0.10.

	Measurements (wt.%)	Average (wt.%)	Standard deviation (wt.%)	Error (wt.%)
C-NPS/Hem$_{0.1}$	6.29 5.77 5.95	6.00	0.26	0.44
C-NPS/Hem$_{0.2}$	12.34 12.77 12.22	12.44	0.29	0.48
C-NPS/Hem$_{0.3}$	18.43 18.11 16.74	17.76	0.9	1.49
C-NPS/Hem$_{0.42}$	22.73 22.64 23.83	23.40	0.66	1.10

Table 5. Average thermal conductivity (W $m^{-1}K^{-1}$) ± standard deviation of the lightweight gypsum composites with different NPS/Hem mass ratio at different temperatures.

Temperature (°C)	C-NPS/Hem$_0$	C-NPS/Hem$_{0.1}$	C-NPS/Hem$_{0.2}$	C-NPS/Hem$_{0.3}$	C-NPS/Hem$_{0.41}$
8	0.369±0.008	0.315±0.004	0.282±0.001	0.260±0.012	0.237±0.009
16	0.362±0.006	0.307±0.005	0.279±0.001	0.254±0.013	0.236±0.009
24	0.359±0.006	0.284±0.007	0.274±0.001	0.245±0.017	0.232±0.009
28	0.356±0.005	0.271±0.006	0.267±0.002	0.240±0.019	0.229±0.010
32	0.354±0.005	0.258±0.004	0.253±0.004	0.236±0.021	0.225±0.011
40	0.346±0.008	0.235±0.004	0.227±0.005	0.220±0.028	0.209±0.018
45	0.337±0.013	0.223±0.004	0.215±0.006	0.208±0.035	0.199±0.024